Eur Biophys J (2004) 33: 310–320
DOI 10.1007/s00249-003-0370-3

ARTICLE

Julie Plastino · Ioannis Lelidis · Jacques Prost
Cécile Sykes

The effect of diffusion, depolymerization and nucleation promoting factors on actin gel growth

Received: 30 September 2003 / Accepted: 14 October 2003 / Published online: 9 December 2003

Abstract In eukaryotic cells, localized actin polymerization is able to deform the plasma membrane and push the cell forward. Depolymerization of actin filaments and diffusion of actin monomers ensure the availability of monomers at sites of polymerization, and therefore these processes must play an active role in cellular actin dynamics. Here we reveal experimental evidence that actin gel growth can be limited by monomer diffusion, consistent with theoretical predictions. We study actin gels formed on beads coated with ActA (and ActA fragments), the bacterial factor responsible for actin-based movement of *Listeria monocytogenes*. We observe a saturation of gel thickness with increasing bead radius, the signature of diffusion control. Data analysis using an elastic model of actin gel growth gives an estimate of 2×10^{-8} cm^{-2} s^{-1} for the diffusion coefficient of actin monomers through the gel, ten times less than in buffer, and in agreement with literature values in bulk cytoskeleton, providing corroboration of our model. The depolymerization rate of actin filaments and the elastic modulus of the gel are also evaluated. Furthermore, we qualitatively examine the different actin gels produced when ActA fragments interact with either VASP or the Arp2/3 complex.

Keywords Actin polymerization · Arp2/3 complex · Lamellipodium · Motility · Vasodilator-stimulated phosphoprotein

Introduction

The polymerization of actin monomers into filaments against a surface drives the extension of cellular lamellipodia, as well as the intracellular movement of certain vesicles and endosomes, and various pathogens. Much progress has been made in the last five years toward understanding the biochemical mechanisms of cellular actin polymerization. Particular emphasis has been placed on the Arp2/3 complex, a component of actin Y-branches (Mullins et al. 1998; Svitkina and Borisy 1999) that is recruited to the leading edge under the control of cellular signaling systems (for review, see Machesky and Insall 1999). The VASP (vasodilator-stimulated phosphoprotein) family proteins also localize to the leading edge of cells, as well as to focal adhesions and stress fibers; however, their role in cell motility is still somewhat controversial (for reviews, see Machesky 2002; Sutherland and Way 2002).

Despite the high concentrations of monomeric actin in cells, filaments do not nucleate spontaneously in vivo owing to the presence of the monomer-binding proteins profilin and thymosin-β4. These two proteins work together to maintain a pool of actin ready to polymerize upon the creation of barbed ends (for review, see Pollard et al. 2000). Owing to the abundance of monomeric actin, diffusion does not seem to limit the polymerization process, although direct experimental evidence is lacking. In fact, the possibility of limitation by diffusion has been suggested theoretically (Noireaux et al. 2000; Mogilner and Edelstein-Keshet 2002), and a recent FLAP (fluorescence localization after photobleaching) study found that diffusion was not sufficient to explain actin delivery to protruding zones in cells (Zicha et al. 2003).

We show here the first experimental evidence that, under certain conditions, diffusion of actin monomers is a limiting factor in the growth of an actin gel. For our study, we took advantage of the well-characterized *Listeria monocytogenes* system, a bacterium that assembles actin filaments at one pole, thereby pushing itself forward within the infected cell. The same proteins as those implicated in leading edge dynamics are involved in this movement: the bacterially produced ActA protein activates actin polymerization nucleation

J. Plastino · I. Lelidis · J. Prost · C. Sykes (✉)
Laboratoire Physicochimie "Curie",
UMR168 Institut Curie/CNRS,
11 rue Pierre et Marie Curie, 75231 Paris cedex 05, France
E-mail: cecile.sykes@curie.fr
Fax: +33-1-40510636

at the *Listeria* surface in association with the Arp2/3 complex (Skoble et al. 2000 and references therein) and VASP (Skoble et al. 2001; Geese et al. 2002 and references therein). Inspired by *Listeria*, our experimental system consists of beads coated with ActA or ActA fragments, placed in cell extracts. Similar systems have already permitted physical studies of actin-based motility in pure protein mixtures (Bernheim-Groswasser et al. 2002), the identification of biochemical partners for actin polymerization (Fradelizi et al. 2001), structural characterizations (Cameron et al. 2001) and the definition of requirements for directional motility (Cameron et al. 1999). Here we use the bead system to compare, in a controlled manner, growing actin gels produced by ActA or fragments of ActA that interact with either VASP or the Arp2/3 complex. With a theoretical analysis of gel thickness data obtained by electron microscopy, we derive the values of three important physical parameters: the diffusion coefficient of actin monomers (D), the rate of depolymerization at filament pointed ends ($k_{\overline{p}}$) and the elastic modulus of the gel (C). VASP-dependent actin network formation is observed for the first time at the microscopic scale.

Materials and methods

Proteins

Glutathione S-transferase (GST) fusions of the N-terminal domain of ActA (NT), amino acids 1–234, and the C-terminal domain (PRO), amino acids 235–584, were prepared as previously described (Golsteyn et al. 1997) and dialyzed into 100 mM borate buffer (pH 8.5). Full-length ActA (amino acids 1–584) equipped with a GST and a 6×his tag was purified as described (Noireaux et al. 2000). Amino acids are numbered according to Kocks et al. (1992).

HeLa cell extracts

HeLa cell extracts were prepared following general guidelines established for platelet extract preparation (Laurent and Carlier 1998). The human HeLa S3 cell line was grown in suspension in Dulbecco's minimal essential medium (DMEM) supplemented with 10% fetal calf serum, under 5% CO_2 at 37 °C. A total of 10^{10} cells were washed twice with PBS and then twice with Wash Buffer (135 mM NaCl, 2.7 mM KCl, 11.9 mM $NaHCO_3$, 0.36 mM NaH_2PO_4, 2 mM $MgCl_2$, 0.2 mM EGTA, 5.5 mM glucose and 0.3% BSA, pH 6.5). Centrifugations were performed at 800×g, for 5–10 min at 4 °C. The wet volume of cells was approximately 20 mL. The cells were then resuspended in 15 mL sonication buffer (10 mM Tris, 10 mM EGTA, 2 mM $MgCl_2$, pH 7.5) with protease inhibitors (Sigma protease inhibitor cocktail for mammalian tissues, diluted 1:100). The cell suspension was passed 10–20 times in a cell cracker at 4 °C in batches of 5 mL, and the homogenate was then centrifuged at 17,000×g for 20 min at 4 °C. The supernatant was transferred to an ultracentrifuge tube; care was taken to avoid the lipid layer floating on the surface. This supernatant was then re-centrifuged at 118,000×g for 1 h at 4 °C. Again care was taken to avoid the grease layer and the solution was supplemented with DTT and ATP to a final concentration of 1 mM each. The total volume of extract was approximately 10 mL. The extract was aliquoted, flash frozen in liquid nitrogen and stored at −80 °C. For actin polymerization reactions, aliquots of extract were thawed, supplemented again with 1 mM ATP, 30 mM creatine phosphate and 1 μM fluorescent actin-Alexa from rabbit muscle (Molecular Probes) and ultracentrifuged at 140,000×g for 10 min at 4 °C. Total protein concentration, as measured by Bradford assay with a BSA standard, after this second ultracentrifugation was about 17 mg/mL.

Characterization of HeLa extracts

The concentrations of actin, the Arp2/3 complex and VASP in HeLa cell extracts were evaluated by quantitative Western blot. For these measurements, extract aliquots were thawed and ultracentrifuged as above, but no supplements were added. Human non-muscle actin (cytoskeleton), bovine Arp2/3 complex and human VASP (kind gifts from Marie-France Carlier) were used as standards. 10% gels of extracts and protein standards were blotted onto nitrocellulose and probed with primary antibodies: monoclonal anti-β-actin (Sigma), monoclonal anti-human VASP (Transduction Laboratories) and polyclonal anti-p41 Arc, a subunit of the Arp2/3 complex. This latter antibody, a gift from Henry Higgs, was made against the C-terminal ten amino acids of human p41 Arc, which is identical in the bovine complex (Robinson et al. 2001). Blots were developed using alkaline phosphatase or the Amplified Opti-4CN detection kit (Biorad). Bands were quantified using the Bio-Profil Imaging System (Vilber Lourmat, France), and standards were fit to a logarithmic curve to calculate protein concentrations in extract samples.

Bead preparation

All beads were purchased from Polyscience. We used polystyrene beads of diameter ranging from 0.5 to 25 μm. Beads were washed twice with borate buffer (100 mM, pH 8.5; Polyscience) before protein coating. A quantity of 0.5–1 nmol of protein in a volume of 10–80 μL was incubated with a total bead surface of about 15 cm^2. The reaction was incubated for 3 h at room temperature with gentle agitation. Beads were resuspended in 50 μL of 10 mg/mL BSA in borate (Polyscience) and incubated for 30 min at room temperature to further ensure that all the bead surface was covered with protein. Beads were then washed and stored in storage buffer (20 mM sodium phosphate, 150 mM NaCl, 10 mg/mL BSA, 0.1% NaN_3, 5% glycerol, pH 7.4; Polyscience) at 4 °C and used within 24 h [note that the proteins are grafted by adsorption onto the bead surface in the current study, whereas covalent attachment was used by Noireaux et al. (2000)].

To measure the protein concentration on the bead surface, a quantity of beads giving about 12 cm^2 total surface was washed in borate buffer, resuspended in SDS sample buffer and heated at 100 °C for 10 min to ensure detachment and denaturation of all proteins. Bead samples were loaded on 7% gels, along with BSA standards. Protein bands were quantified by comparison to BSA standards using the Bio-Profil Imaging System. Protein amounts were converted to density values by taking into account the exact surface area of beads loaded on the gel and using the following molecular weights: GST-ActA-His, 90 kDa; GST-NT, 52 kDa; and GST-PRO, 64 kDa. All three proteins were at maximal surface concentration, corresponding to a distance between protein molecules on the surface of 16.9 ± 3.5 nm for ActA-coated beads, 7.5 ± 0.9 nm for NT-coated beads and 8.9 ± 1.5 nm for PRO-coated beads.

Fluorescence microscopy of beads

VASP recruitment to bead surfaces was evaluated by incubating 0.5 μm radius beads in extract treated with 5 μM latrunculin A (Molecular Probes) to prevent actin polymerization. The reaction was incubated at room temperature for 30 min, before being probed with monoclonal anti-human VASP (Transduction Laboratories) and then with Texas Red secondary antibody (Santa Cruz

Biotechnology). For the control reaction, the primary antibody was omitted. Beads were imaged at 100 times magnification on an Olympus inverted microscope equipped with an intensified CCD camera (Lhesa, France). All images were taken at identical exposure, and fluorescence intensities at bead surfaces were quantified using Metamorph software (Universal Imaging). At least 10 beads were evaluated for each measurement, and the background next to each bead was subtracted.

To observe actin treadmilling over time, we acquired images (1 s exposure) every 5 min with a Leica inverted microscope equipped with a CCD camera (Princeton Instruments), and fluorescence intensities were quantified as above.

Reactions for electron microscopy

For reactions using beads of different sizes, it is important that the total surface area for actin polymerization remain constant. Derivatized beads at a total bead surface of 0.83 cm^2 (for example, 4.94 μL of 9.634 μm beads at a concentration of 2.7%) were washed in 50 mM phosphate buffer (pH 6.3) and then resuspended in 50 μL prepared HeLa extract. Reactions were incubated at room temperature for 4 h without agitation. Beads were pelleted in a horizontal centrifuge at 2000×*g* for 10 min at room temperature. The pellet surface was washed twice with cold CB buffer (10 mM MES, 150 mM NaCl, 5 mM EGTA, 5 mM $MgCl_2$, 5 mM glucose, pH 6.1), and processed immediately for epon inclusion.

Epon inclusion and electron microscopy

Washed bead pellets were fixed in glutaraldehyde and tannic acid, rinsed with buffer, post-fixed with osmium, water washed and stained with 2% uranyl acetate as previously described (Noireaux et al. 2000), except that, for all steps, CB buffer was substituted for phosphate buffer. Samples were then dehydrated in alcohol and embedded in epon. Ultrathin sections (80 ± 10 nm) were stained for 20 min with 4% uranyl acetate, washed three times with water and then incubated for 1–3 min in lead citrate. Grids were analyzed on a Philips CM 120 electron microscope at 80 kV. Gel thicknesses on bead surfaces were measured using Metamorph software. Thickness measurements were performed on beads that had been sectioned through the center, and each thickness represents the average of at least 10 beads chosen at random.

Results

Actin filaments accumulate around beads coated with ActA and ActA variants

Three constructs of the ActA protein of *Listeria* are studied: full-length ActA, the N-terminal domain of ActA (NT), which binds Arp2/3, and the C-terminal domain of ActA (PRO), which binds VASP. When these proteins are adsorbed onto the surface of polystyrene beads and incubated in HeLa cell extracts doped with fluorescently labeled actin monomer, symmetrical actin clouds are observed around all three types of beads by fluorescence microscopy, as already described by Noireaux et al. (2000) for ActA and by Fradelizi et al. (2001) for PRO and a homologue of NT (VCA). Plastic embedding and thin sectioning, followed by observation by electron microscopy, confirms the presence of filamentous actin around the beads. As shown in Fig. 1a–c for 7.9 μm radius beads, the three ActA constructs produce different actin structures at the surface of the beads. The NT-produced gel is a loose, fragmented meshwork, while the gel generated by full-length ActA is denser and more regular. PRO-coated beads interact with VASP, as shown by immunofluorescence (Fig. 2). These beads produce a tight dense actin gel, unlike control beads coated with BSA that do not show any actin accumulation at the surface (Fig. 1d). We rarely observe comet formation in these experiments, but with platelet extracts, beads coated with either ActA or NT display actin comets, although no movement is detected for beads coated with PRO (J. Plastino, unpublished results). In this paper, we focus on spherical gel growth in HeLa cell extracts only. These extracts contain

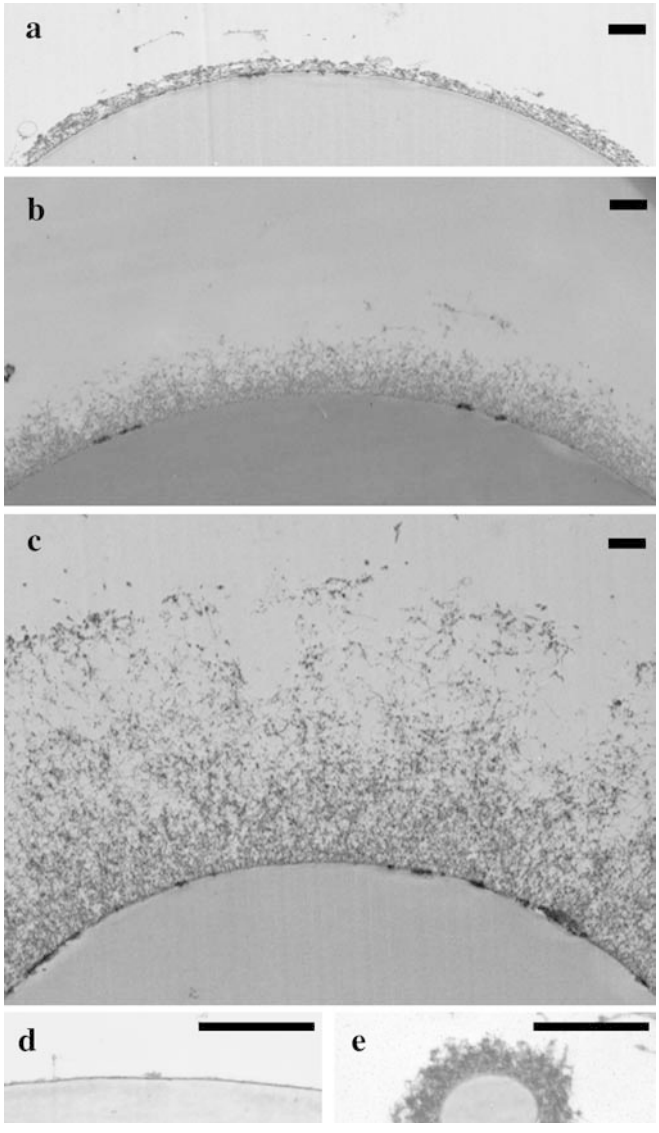

Fig. 1a–e Electron microscopy of thin sections of beads supporting a steady-state actin layer. Before incubation in cell extracts, beads are coated with an actin polymerization activator protein: (**a**) PRO, (**b**) ActA, (**c**) and (**e**) NT. (**a**)–(**c**) represent 7.9 μm radius beads; (**e**) is a 0.3 μm radius bead; (**d**) is the negative control: a 4.6 μm radius BSA-coated bead. Note the large open zones in the NT-produced gel on the 7.9 μm radius bead (**c**). *Bar*: 500 nm

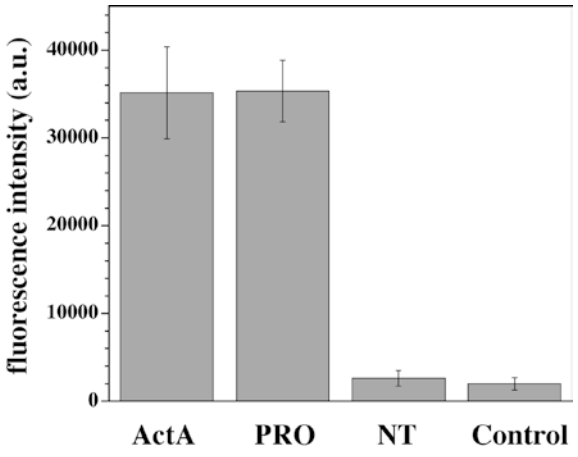

Fig. 2 Quantification by immunofluorescence of VASP recruitment to bead surfaces. ActA-, PRO- and NT-coated beads are incubated in cell extracts treated with latrunculin A, and then probed with an antibody directed against VASP, followed by a fluorescent secondary antibody. The control represents beads treated exclusively with secondary antibody. Average fluorescent intensities of the beads are shown in arbitrary units (a.u.). PRO-coated beads bind VASP just as well as full-length ActA-coated beads, while NT-coated beads are indistinguishable from the control, as expected

4 ± 1 μM actin, 11 ± 3 μM Arp2/3 and 50 ± 20 nM VASP (Table 1). Under our reaction conditions (see Materials and methods), actin and Arp2/3 are, thus, in large excess over nucleation activator on the bead surface, and VASP is present in approximately stoichiometric amounts.

Dependence of gel thickness on bead size

As seen in Fig. 1, the three different proteins produce actin accumulations of different thicknesses. Increasing the reaction time from 4 to 6 hours for the ActA and PRO beads does not augment the observed thickness, indicating that the smaller thickness observed with these proteins is not due to different speeds of accumulation. In addition, incubating the beads in a larger amount of extract or adding more extract at 4 h does not appreciably change the observed thickness, so the lack of further growth is not due to a depletion of extract components. Therefore we conclude that the thicknesses observed in Fig. 1 represent the steady state of a treadmilling population of actin filaments: polymerization is still occurring at the barbed ends at the bead surface but it is balanced by depolymerization at the outer surface of the gel. Treadmilling of the actin cloud around ActA beads is confirmed by adding fluorescent actin to bead reactions run in the absence of fluorescent label for 6 hours. We observe by video microscopy that fluorescence is incorporated into the actin cloud, fully recovering the fluorescence observed around control beads (Fig. 3) (Noireaux 2000).

From these observations, we can state that the stationary gel thickness is dependent on the nature of the protein on the surface of the bead. Furthermore, we find that, within a series of beads all coated with the same protein at the same surface density, the steady-state gel thickness is dependent on bead size. A complete profile of gel thickness as a function of bead radius for ActA-,

Table 1 Definition of symbols and summary of associated values

Symbol	Value	Meaning	Reference
Not used	4 ± 1 μM	Actin concentration in HeLa extracts	Measured in this paper
Not used	11 ± 3 μM	Arp2/3 concentration in HeLa extracts	Measured in this paper
Not used	50 ± 20 nM	VASP concentration in HeLa extracts	Measured in this paper
k_+^b	11.6 μM^{-1} s^{-1}	Barbed end assembly rate constant	(Pollard 1986)
k_-^b	1.4 s^{-1}	Barbed end disassembly rate constant	(Pollard 1986)
k_-^p	0.27 s^{-1}	Pointed end disassembly rate constant	(Pollard 1986)
	0.06 ± 0.02 s^{-1}	Pointed end disassembly rate constant in an ActA-produced gel, estimated from model	Estimated in this paper
c_e	0.4 μM	Monomeric actin available for polymerization, based on critical concentrations	Critical concentrations barbed (0.12 μM) and pointed ends (0.60 μM) (Pollard 1986)
	0.27 ± 0.03 μM	Monomeric actin available for polymerization, estimated from model	Estimated in this paper
a	2.75 nm	Filament length gained per monomer	Estimation based on (Holmes et al. 1990)
l_p	15 μm	Persistance length of an actin filament	(Isambert et al. 1995; Käs et al. 1996) and references therein
ξ	23–36 nm	Spacing between barbed ends in the lamellipodia of migrating fibroblasts	1370 ± 578 ends/μm^2 (Abraham et al. 1999)
	16.9 ± 3.5 nm	Spacing between barbed ends at the surface of an ActA-coated bead	Measured in this paper (ActA surface density)
D	3.1×10^{-8} cm^{-2} s^{-1}	Diffusion coefficient of actin monomer in bulk cytoskeleton	(McGrath et al. 1998)
	2×10^{-8} cm^{-2} s^{-1}	Diffusion coefficient of actin monomer in an ActA-produced gel	Estimated in this paper
δ	≤ 52 nm	Pore size in the cytoplasmic actin gel of Swiss 3T3 cells	(Luby-Phelps et al. 1987)
	53 nm	Pore size of an ActA-produced actin gel	Estimated in this paper
C	10^3–10^4 Pa	Elastic modulus of *Listeria* comet tail	(Gerbal et al. 2000)
	8×10^3 Pa	Elastic modulus of ActA-produced actin gel	Estimated in this paper

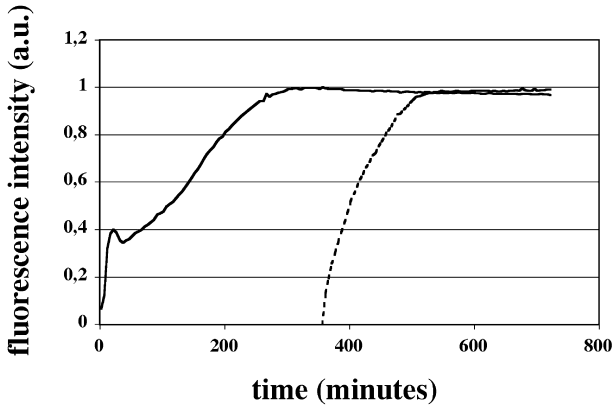

Fig. 3 Demonstration of treadmilling in actin clouds around beads. 5 μm radius beads coated with ActA are incubated in cell extracts, and the increase of fluorescence (arbitrary units) around the beads is monitored over time (minutes). The *solid line* depicts the profile obtained when the cell extracts contain fluorescently marked monomeric actin at time 0. The *dashed line* represents a bead incubated in extracts lacking fluorescent actin for 6 h. Extract containing fluorescent marker is then added, and as expected in a treadmilling situation, fluorescent signal is incorporated into the actin gel around the bead. The two curves are normalized to a maximum fluorescent signal of 1

NT- and PRO-coated beads is shown in Fig. 4. These data are also summarized in Table 2.

ActA-coated beads, with radii r of up to 5 μm, display gel thicknesses proportional to r; however, for larger beads ($r > 5$ μm), the gel thickness becomes independent of the bead radius. The implications of this profile and the contribution of diffusion will be explained more thoroughly in the next section. For NT-coated beads, the dependence of gel thickness on bead radius does not level off at larger bead sizes. The standard deviation bars for larger beads coated with NT reflect the increasing irregularity of the actin gel; large open zones are apparent around these beads, whereas for smaller beads the gel is more homogenous (Fig. 1e). For 10.7 and 12.45 μm radius beads, the gels are too irregular to allow for thickness measurements. For PRO-coated beads, the thickness of the actin gel for beads of less than 2 μm in radius cannot be measured owing the small amount of actin around these beads. However, we can still observe that the PRO-generated gel thicknesses augment with larger bead sizes, reaching a plateau value of about 300 nm.

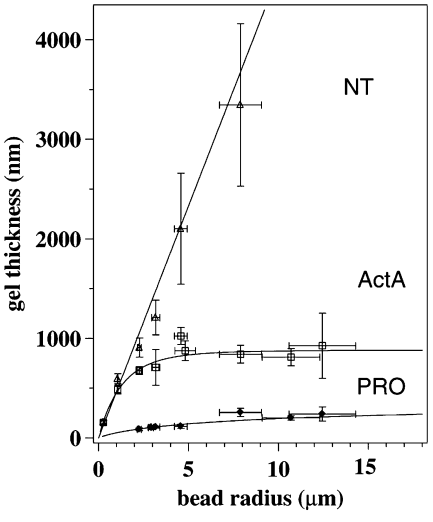

Fig. 4 Gel thickness data as a function of bead size for NT- (*open triangles*), ActA- (*open squares*) and PRO-coated beads (*filled diamonds*) incubated in HeLa cell extracts. For ActA and PRO, *solid lines* represent the fits obtained using Eq. (9). For the ActA-produced gel, the parameters e_0^*, ω_1, ω_2 and ω_3 are generated by the fit, and D and C are calculated from e_0^* and ω_3, respectively. For the PRO-produced gel, ω_1 and ω_2 are fixed to the values obtained for the ActA data fit, but e_0^* and ω_3 are left free, and D and C are calculated accordingly. The linear increase for NT-beads data corresponds to a regime in which the open zones in the gel may allow more rapid diffusion of actin monomers to the bead surface

Evaluation of actin gel properties by modeling gel thickness dependence on bead size

As seen in Fig. 4, ActA-coated beads, with radius r ranging from 0.25 to 5 μm, support steady-state actin gel thicknesses proportional to r as previously described and theoretically modeled (Noireaux et al. 2000). Interpretation of these results recognized the elastic properties of the actin gel. Because the actin filaments grow from a spherical surface, the actin gel has to deform to let monomers insert between the gel and the surface. This stretches the cross-linked gel, creating a stress orthogonal to the surface of the bead that prevents further addition of monomers, and a tangential stress that pulls on the outer gel layer and triggers fractures (σ_{ortho} and σ_{tang}, Fig. 5). The spherical constraint is less pronounced for beads of larger radii because they more closely approximate a flat surface, and consequently these beads display thicker gels.

It is predicted by Noireaux et al. (2000) that the gel thickness for larger ActA-coated beads will be limited by monomer diffusion. This effect is seen in Fig. 4, where the gel thickness becomes independent of the bead radius for $r > 5$ μm. In this diffusion-limited regime, the thickness of the gel around the bead is such that it impedes the arrival of actin monomers at the surface. As a result, a radius-independent steady state is reached where diffusion to the bead surface followed by polymerization is balanced by depolymerization at the outer surface of the gel. Note that the current data set is not superimposable with the experiments of Noireaux et al. (2000) owing to both a different ActA grafting method (see Materials and methods) and an improvement in the extract preparation. In fact, the cell extracts in our study are 50% higher in total protein. This concentration difference could affect the polymerizing activity of the extracts, as has been observed with cell extracts from *Xenopus* eggs and platelets (Laurent and Carlier 1998; Theriot and Fung 1998). Nevertheless, the current and former data sets can be treated with the same theoretical analysis.

Table 2 Actin gel thickness as a function of bead radius for ActA-, NT- and PRO-coated beads

Bead radius (μm)	Actin thickness (nm)		
	ActA-coated beads $\xi = 16.9 \pm 3.5$ nm[a]	NT-coated beads $\xi = 7.5 \pm 0.9$ nm	PRO-coated beads $\xi = 8.9 \pm 1.5$ nm
0.264 ± 0.005	156 ± 16	161 ± 18	n.d.
1.067 ± 0.020	488 ± 43	595 ± 51	n.d.
2.269 ± 0.118	676 ± 38	n.d.	86 ± 13
2.281 ± 0.105	n.d.	907 ± 96	n.d.
2.916 ± 0.137	n.d.	n.d.	105 ± 20
3.174 ± 0.228	710 ± 181	1209 ± 174	109 ± 9
4.570 ± 0.355	1025 ± 85	2101 ± 559	117 ± 21
4.817 ± 0.569	877 ± 98	n.d.	n.d.
7.90 ± 1.17	842 ± 89	3347 ± 816	256 ± 42
10.70 ± 1.61	812 ± 87	n.d.	201 ± 22
12.45 ± 1.85	927 ± 327	n.d.	240 ± 70

[a] ξ is the distance between protein molecules on the surface of the bead (see Materials and methods section). All thickness and ξ values are represented as averages ± the standard deviation, and are shown unrounded, as used to generate the plots in Fig. 4. Errors on the bead radii are provided by the manufacturer. n.d. = not determined.

Diffusion can be evaluated by fitting the thickness data as a function of bead size, as follows. We use the general equation (Eq. 1) to describe the growth of an actin gel on a spherical surface. This equation is obtained as in Noireaux et al. (2000) by writing that depolymerization at the outer surface of the actin gel balances the polymerization at the inner surface, the actin monomers being transported by diffusion. We note D, the diffusion coefficient of actin monomers within the gel, e, the actin gel thickness for a bead of radius r, and c_e, the concentration of actin monomers available for polymerization in the cell extract, considered as constant outside the actin gel region:

$$c_e k_+^{\mathrm{b}}(\sigma_{\mathrm{ortho}}) \left[1 - \frac{e/e^*(\sigma_{\mathrm{tang}})}{1 + e/r} \right] = k_-^{\mathrm{b}}(\sigma_{\mathrm{ortho}}) + k_-^{\mathrm{p}}(\sigma_{\mathrm{tang}}) \tag{1}$$

We consider polymerization and depolymerization at the interior and exterior surfaces of the gel only, and neglect depolymerization in the body of the gel. This assumption appears true for ActA- and PRO-coated beads, which display essentially homogeneous gels, but not for NT-coated beads where the outer part of the gel body appears holey. k_-^{p} is the depolymerization rate at the pointed end, taken as a constant by Noireaux et al. (2000). Here, we take into account the dependence of k_-^{p} upon the tangential stress σ_{tang}, a reasonable addition to the model since the gel is stretched at the outer surface. k_+^{b} and k_-^{b} are the polymerization and depolymerization rates at the barbed end, respectively, and are dependent upon the orthogonal stress, σ_{ortho}. The expression for $e^*(\sigma_{\mathrm{tang}})$ is:

$$e^*(\sigma_{\mathrm{tang}}) = \frac{D\xi^2 c_e}{k_-^{\mathrm{p}}(\sigma_{\mathrm{tang}})} \tag{2}$$

and represents the characteristic gel thickness for which diffusion becomes the limiting factor in gel polymerization; ξ is the distance between nucleation promoting proteins on the surface of the bead, or in other words the distance between actin filaments polymerizing at the bead surface. When rearranged to give a description of gel thickness in terms of bead radius, and noting $x = e/r$, Eq. (1) gives:

$$x = \frac{e^*(\sigma_{\mathrm{tang}})}{r} \times (1 + x) \times \left[1 - \frac{k_-^{\mathrm{b}}(\sigma_{\mathrm{ortho}}) + k_-^{\mathrm{p}}(\sigma_{\mathrm{tang}})}{c_e k_+^{\mathrm{b}}(\sigma_{\mathrm{ortho}})} \right] \tag{3}$$

Given that x is smaller than 1, the tangential component of the stress can be expressed by: $\sigma_{\mathrm{tang}} = Cx$ (Landau and Lifchitz 1976), where C is the elastic modulus of the gel. Writing the equilibrium equation for the stress distribution as done by Noireaux et al. (2000) gives $\sigma_{\mathrm{ortho}} = Cx^2$. The stress-dependent rates k_+^{b}, k_-^{b} and k_-^{p} follow a Boltzmann law, as described by Kramers and Eyring rate theory (Eyring 1935; Kramers 1940); $\xi^2\sigma$ is the force acting on association or dissociation of a monomer to/from a filament, and a is the distance over which the force is applied, i.e. the filament length gained per actin monomer; k_{B} and T are the Boltzmann constant and the temperature, respectively, and:

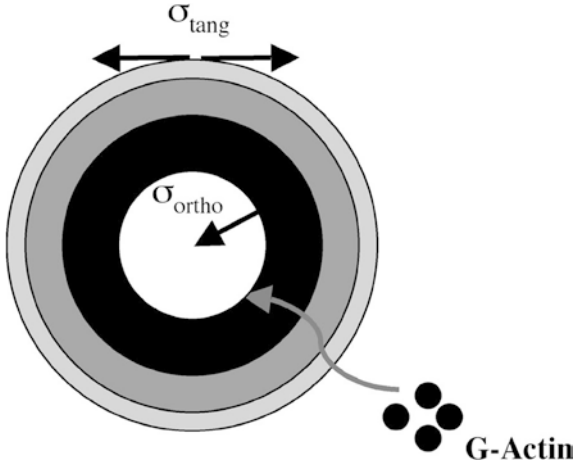

Fig. 5 Growth of an actin gel on a spherical surface. Actin polymerization occurs at the surface of the bead after diffusion of actin monomers through the actin gel to filament barbed ends. Tangential (σ_{tang}) and orthogonal (σ_{ortho}) stress is created due to the stretching of the *light gray* layers over the newly formed *black* layer of F-actin. This stress effect would not exist on a flat surface

$$\omega_3^2 = \frac{2k_BT}{a\,\xi^2\,C} \tag{4}$$

$$k_+^b(\sigma_{ortho}) = k_+^b(0)\exp\left[-\frac{a\,\xi^2\,\sigma_{ortho}}{2k_BT}\right] = k_+^b(0)\exp\left[-\frac{a\,\xi^2\,C}{2k_BT}x^2\right] = k_+^b(0)\exp\left[-\frac{x^2}{\omega_3^2}\right] \tag{5}$$

$$k_-^b(\sigma_{ortho}) = k_-^b(0)\exp\left[\frac{a\,\xi^2\,\sigma_{ortho}}{2k_BT}\right] = k_-^b(0)\exp\left[\frac{a\,\xi^2\,C}{2k_BT}x^2\right] = k_-^b(0)\exp\left[\frac{x^2}{\omega_3^2}\right] \tag{6}$$

For the stress dependence of k_-^p, it is useful to take into consideration the stretching of the gel. From geometrical considerations, the distance between filaments at the exterior of the gel (ξ_e) equals $\xi(1+x)$. The force acting on a single filament $\xi_e^2\,\sigma_{tang}$ is therefore equal to $\xi^2C(x+2x^2)$, neglecting the third-order term. This gives the following expression for k_-^p:

$$k_-^p(\sigma_{tang}) = k_-^p(0)\exp\left[\frac{a\xi_e^2\sigma_{tang}}{2k_BT}\right] = k_-^p(0)\exp\left[\frac{a\xi_e^2C}{2k_BT}(x+2x^2)\right] = k_-^p(0)\exp\left[\frac{x+2x^2}{\omega_3^2}\right] \tag{7}$$

e^* then reads:

$$e^*(\sigma_{tang}) = \frac{D\xi^2c_e}{k_-^p(\sigma_{tang})} = \frac{D\xi^2c_e}{k_-^p(0)}\exp\left[-\frac{x+2x^2}{\omega_3^2}\right] \tag{8}$$

The presence of the factor 1/2 in the expressions for both depolymerization and polymerization (Eqs. 5, 6, 7) assumes that the force affects on and off rates equally at the barbed and pointed ends. We tested this assumption by radically changing the value of this factor to 1 and 0 for polymerization and depolymerization, respectively. This did not appreciably change the results of the fit. Moreover, equal effects of force on polymerization and depolymerization have been shown to be reasonable for microtubules, although the dominant effect is nevertheless ascribed to a reduction in the on rates (Dogterom and Yurke 1997).

Combining Eqs. (3) and (5, 6, 7, 8) gives Eq. (9):

$$e = e_0^*\exp\left[-\frac{x+2x^2}{\omega_3^2}\right]\times(1+x)\times\left\{1-\omega_2\exp\left[2\frac{x^2}{\omega_3^2}\right]-\omega_1\exp\left[\frac{x+3x^2}{\omega_3^2}\right]\right\} \tag{9}$$

where:

$$e_0^* = \frac{D\xi^2c_e}{k_-^p(0)},\quad \omega_1 = \frac{k_-^p(0)}{c_ek_+^b(0)}\quad\text{and}\quad \omega_2 = \frac{k_-^b(0)}{c_ek_+^b(0)} \tag{10}$$

This is a complete description of gel thickness as a function of bead radius that takes into consideration the stress-dependent rates of polymerization at the barbed end and depolymerization at the barbed and pointed ends, the spacing between nucleation promoting proteins on the bead surface, the diffusion coefficient for actin monomer through the actin gel, and the external monomer concentration.

As starting parameters for the fit (see Table 1), the stress-free values for k_+^b, k_-^b and k_-^p are taken as 11.6 $\mu M^{-1}\,s^{-1}$, 1.4 s^{-1} and 0.27 s^{-1}, respectively (Pollard 1986). c_e is defined as 0.4 μM or 2.4×10^{14} molecules/cm^3, because it is intermediary between the critical concentrations of the barbed and pointed ends, 0.12 μM and 0.60 μM, respectively (Pollard 1986). These parameters give input values for the fit of $\omega_1\approx0.06$ and $\omega_2\approx0.3$; ω_3 is loosely defined as 0.1–10, with the assumptions that a is in the nm range, ξ is in the tens of nm range and C is in the range 10^3–10^6 Pa. e_0^* is taken to be on the order of 1 μm. All four fitting parameters are left free during the fit.

For the ActA data, a Levenberg–Marquardt nonlinear least-squares fitting routine generates the values for e_0^*, ω_1, ω_2 and ω_3, as shown in Table 3. To reduce adjustable parameters, the fit for the PRO data is obtained using parameters ω_1 and ω_2 as already defined for ActA data, since less experimental data are available for the PRO-coated beads. This assumption implies that the stress-free values for k_+^b, k_-^b and k_-^p are similar in ActA- and PRO-produced gels. For k_+^b and k_-^b this is a valid assumption because these parameters are diffusion limited (Drenckhahn and Pollard 1986), and therefore cannot be further augmented by interaction with the bead surface. For k_-^p, the pointed ends of the filaments are not close to the surface, and therefore k_-^p is unlikely to be directly affected by the nucleation promoting protein. However, by recruiting different cross-linking and bundling proteins to the actin gel, the activator protein on the bead could indirectly alter k_-^p, and, in this case, the ω_1 found for the ActA data fit would not be appropriate for PRO. Yet the fit for the PRO data is reasonable, sustaining the use of ActA parameters for this analysis.

The difference between the input values for ω_1 and ω_1 and the ones generated by the fit indicates that some of the initial values of $k_+^b(0)$, $k_-^b(0)$ or c_e are not appropriate to our experimental situation. This disparity is normal, considering that the initial values are taken from purely in vitro estimations while our experiments are performed in cell extracts that contain proteins capable of altering the rate constants of actin assembly. As noted above, $k_+^b(0)$ and $k_-^b(0)$ cannot be further increased since their values correspond to diffusion-limited processes. We therefore use ω_1 and ω_1 to recalculate the values of $k_-^p(0)$ and c_e, parameters known to be affected by ADF/cofilin and capping proteins present in the cell (for review, see Carlier 1998). c_e is recalculated from ω_1 to give 0.27 ± 0.03 μM, still intermediary between the critical concentrations of the barbed and pointed ends.

Table 3 Fit parameters and results for ActA- and PRO-produced actin gels

Nucleation promoting factor	e_0^*(μm)	ω_1	ω_2	ω_3	D (cm^2/s)[a] average (range)	C (Pa)[a] average (range)
ActA	1.6 ± 0.1	0.020 ± 0.005	0.45 ± 0.05	1.2 ± 0.1	2×10^{-8} ($1–6\times10^{-8}$)	8×10^3 ($2–15\times10^3$)
PRO	0.7 ± 0.1			0.19 ± 0.02	3×10^{-8} ($1–9\times10^{-8}$)	1×10^6 ($0.6–1.9\times10^6$)

[a]Diffusion coefficients (D) and gel elastic moduli (C) are calculated using ξ values of 16.9 ± 3.5 nm and 8.9 ± 1.5 nm for the distance between ActA and PRO proteins on the surface of the beads, respectively. For calculating D, we use $k_-^p(0)$equal to 0.06 ± 0.02 s^{-1} and c_e equal to $1.6 \pm 0.2\times10^{14}$ molecules/cm^3, as derived from the fitting parameters ω_1 and ω_2. Values are represented as ± one standard deviation or as averages with upper and lower limits in parentheses

This value of c_e and ω_1 give $k_-^p(0)$ values of 0.06 ± 0.02 s^{-1}, about five times less than the measured value in vitro.

The fitting procedure gives e_0^* values of 1.6 ± 0.1 and 0.7 ± 0.1 μm for the curves corresponding to ActA-coated beads and PRO-coated-beads, respectively. To calculate D, we use the expression:

$$e_0^* = \frac{D\xi^2 c_e}{k_-^p(0)} \tag{11}$$

with adjusted values for $k_-^p(0)$ and c_e ($c_e = 0.27 \pm 0.03$ μM $= 1.6 \pm 0.5\times10^{14}$ cm^{-3}). The ξ values measured by SDS-PAGE (Fig. 6 and Materials and methods) for ActA and PRO adsorption to the bead surface are 16.9 ± 3.5 nm and 8.9 ± 1.5 nm, respectively, giving average D values of 2×10^{-8} cm^2/s (with a range of $1–6\times10^{-8}$ cm^2/s) for actin monomers in the ActA-produced gel and 3×10^{-8} cm^2/s (with a range of $1–9\times10^{-8}$ cm^2/s) for actin monomers in the PRO-produced gel.

The elastic moduli (C) for the gels formed around ActA and PRO beads are calculated from the values of ω_3 generated by the fit (see Table 3) and:

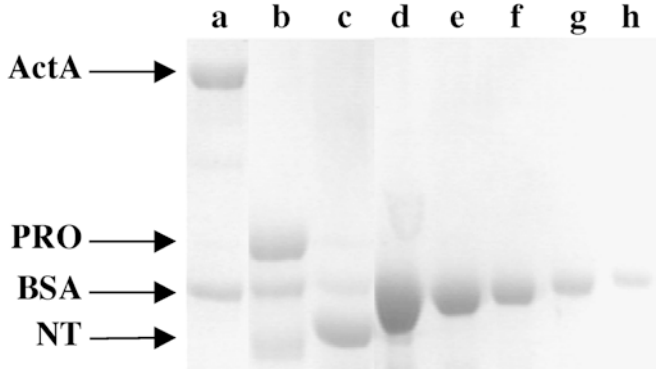

Fig. 6 Quantification of actin polymerization promoting factors on bead surfaces for the determination of the spacing (ξ). Beads coated with (*a*) ActA, (*b*) PRO and (*c*) NT and subsequently with BSA (as described in Materials and methods) are heated in sample buffer to release proteins from the bead surfaces, separated on a 7% polyacrylamide gel, and stained with Coomassie. Protein amounts are calculated by comparing the band intensities for ActA, PRO and NT (indicated by *arrows*) to a BSA standard curve: (*d*) 5, (*e*) 2.5, (*f*) 1.25, (*g*) 0.63 and (*h*) 0.31 μg

$$\omega_3^2 = \frac{2k_B T}{a\,\xi^2\,C} \tag{12}$$

$k_B T$ at room temperature is equal to 4.1×10^{-21} N m, and the ξ values for ActA and PRO beads are as for the calculation of D. The value of a is defined as half of an actin monomer or 2.75 nm: actin monomers polymerize with their large dimension of 5.5 nm parallel to the filament axis (Holmes et al. 1990), but since the filament is a double helix, each monomer only adds 2.75 nm to the length of the filament. We find gel elasticities of 8×10^3 Pa (with a range of $4–15\times10^3$ Pa) in the case of the ActA-produced gel, and 1×10^6 Pa (with a range of $0.6–1.9\times10^6$ Pa) for the gel formed around the PRO-coated beads. These values and the reasonable assumption for dimensional arguments that C depends on the mesh size (δ) of the gel by the relation:

$$C \approx \frac{k_B T l_p}{\delta^4} \tag{13}$$

(Gerbal et al. 1999) allow us to estimate the value of δ for the gels produced by the two nucleation activators. With the persistence length of an actin filament (l_p) approximately equal to 15 μm (Isambert et al. 1995; Käs et al. 1996 and references therein), the mesh sizes are 53 nm for the ActA-produced gel and 16 nm for the PRO-produced gel.

As shown in Fig. 4, the NT-coated beads behave in a very different manner: the gel thickness dependence on the radius is linear with no sign of leveling off, and, on large beads, the gels are much thicker than for the other two nucleation promoting proteins. Although the NT-produced actin gel is uneven around large beads (Fig. 1c), it is more regular for smaller beads (Fig. 1e), and we can therefore use the slope of the linear fit to give an approximation of the elastic modulus of the NT-produced gel, as follows. The slope is related to the elastic modulus C by the formula:

$$\frac{e}{r} = \sqrt{\frac{\Delta\mu}{C\,\xi^2\,a}} \tag{14}$$

(Noireaux et al. 2000), where $\Delta\mu$ [about $14k_B T$ (Gordon et al. 1976)] is the chemical energy released in the polymerization process, and ξ and a are as previously defined. The slope of the linear fit to the NT data in Fig. 4 is 0.47 ± 0.02. With ξ equal to 7.5 ± 0.9 nm, this

gives an estimate for C on the order of $1–24\times10^5$ Pa, comparable to that for the PRO-produced gel.

Discussion

Actin gels on spherical surfaces

Our work on actin gels grown from the surface of beads has two main objectives. One is to study the effect of nucleation promoting proteins on the physical properties of the actin gel. The other is to test the elastic model by using it to estimate important parameters that govern gel growth: the diffusion coefficient of actin monomers, the rate of depolymerization at filament pointed ends, and the elastic modulus of the actin gel. To address the first question, we examine gel thicknesses for beads coated with ActA and with the ActA fragments PRO and NT. Because the C-terminal portion of ActA (PRO) binds VASP and the N-terminal part of ActA (NT) binds the Arp2/3 complex, these fragments allow us to separate the action of VASP and the Arp2/3 complex on actin assembly, and compare their individual activities. This study represents the first microscopic observation of VASP-dependent actin gel formation.

We show that the symmetrical gels generated by ActA and the fragments of ActA display different thickness profiles in relation to bead size (Fig. 1, Fig. 4 and Table 2). However, for all three variants, very small beads support a thinner actin layer than larger beads, a phenomenon due to the elastic properties of the actin gel, as explained in the Results section and in Fig. 5. For ActA- and PRO-coated beads, the gel thickness is constant for large beads because the diffusion of monomers to the surface of the bead is the limiting factor in gel growth (Results section). The curves for ActA- and PRO-gel thickness as a function of bead radius in Fig. 4 can be explained by a stress-limited regime followed by a diffusion-limited situation. The diffusion-limited regime is not observed for the NT-produced gel in the range of bead sizes used in this study, and the thickness measurements on larger bead sizes are impossible due to the high heterogeneity of the gel (Fig. 1c). The fact that these anfractuosities are absent from ActA- and PRO-produced gels suggests that VASP could prevent gel breaking. The interplay of VASP that produces unbranched filaments (Bear et al. 2002) and Arp2/3 that gives branched filaments could be important for a cohesive actin gel.

ActA-, PRO- and NT-produced actin gel properties from thickness measurements

By fitting the complete data set of gel thickness as a function of bead size, we are able to calculate several important parameters for the ActA-produced actin gel: the diffusion coefficient of actin monomer (D), the elastic modulus of the ActA-produced gel (C), and the rate of actin filament depolymerization at the pointed end [$k_-^p(0)$]. See Table 1 for a summary of literature and calculated values. Our estimation for D of 2×10^{-8} cm^2/s is similar to the value previously measured by PAF (photoactivation of fluorescence) in the bulk cytoskeleton of subconfluent endothelial cells: $3.1\pm0.4\times10^{-8}$ cm^2/s (McGrath et al. 1998). The diffusion coefficient of G-actin in low-salt buffer is $7.15\pm0.35\times10^{-7}$ cm^2/s (Lanni and Ware 1984). Adjusting for the four times higher viscosity of the fluid phase of cytoplasm (Luby-Phelps et al. 1986), the diffusion coefficient of actin monomer in cells or cell extract is expected to be about 1.8×10^{-7} cm^2/s. This estimate is ten times greater than what we actually find in ActA-produced actin gels.

In order to interpret this difference, we estimate the mesh size of the actin gel (δ) using the elastic modulus value C. For the ActA gel, we find $C=8\times10^3$ Pa, in agreement with previous measurements of the elasticity of *Listeria* comet tails (Gerbal et al. 2000). From this, we estimate the pore size of the actin gel at 53 nm, consistent with measurements in cells (Luby-Phelps et al. 1987). With an actin monomer size of $3.5\times5.5\times5.5$ nm^3 (Kabsch et al. 1990) and a pore size of 53 nm, actin monomer diffusion should not be mechanically impeded by the actin meshwork. The ten-fold reduction in diffusion of actin through the actin gel suggests, therefore, that monomers interact with the actin network during their diffusion to the barbed ends, and may attach temporarily to the network, thus slowing their diffusion. In theory, the calculated D could represent the diffusion of another protein, for example, both the Arp2/3 complex and VASP are recruited by ActA to the filament barbed ends. The size of the Arp2/3 complex is on the order of $15\times14\times7–10$ nm^3 (Robinson et al. 2001), and VASP has a similar molecular weight to actin [46 kDa (Reinhard et al. 1992)]. Since 90–97% of the diffusion space must be occluded in order to substantially reduce diffusion (Ölveczky and Verkman 1998), both of these molecules are expected to diffuse through the gel unhindered, although, like actin, their motion could be slowed by temporary attachments to the actin network. However, given the reasonable values we obtain for D [in accordance with the results of McGrath et al. (1998)], as well as for C, it is unlikely that we mistakenly measured the diffusion coefficient of some other species.

The fitting parameters ω_1 and ω_2 give us a novel way to evaluate the rate of actin filament depolymerization at the pointed end [$k_-^p(0)$]. One would expect this parameter to be enhanced from its in vitro value of 0.27 s^{-1} by the action of actin depolymerizing factors in the HeLa cell extract. Instead, we find a $k_-^p(0)$ value of 0.06 s^{-1}, five times smaller than the in vitro value. A likely explanation for this small value is that the in vitro measurements were performed on solitary filaments, while, in the gel around the beads, the actin filaments are associated into a network by various bundling, cross-linking and branching factors in the cell extracts. The association points created by these factors may impede the depolymerization of pointed ends. In the same cell extract used for our experiments, another estimate of

$k_-^p(0)$ is found to be even lower: 1 μm beads coated with VCA, the Arp2/3-interacting portion of WASP, display actin comets 10.5 μm in length with the beads moving at speeds of 3.4 μm/min (A. Bernheim-Groswasser, unpublished results). By the ratio of velocity to length (Theriot et al. 1992), we calculate a $k_-^p(0)$ value of 0.005 s^{-1}, 50 times smaller than the in vitro value. This difference could again be due to the different amount of branches and cross-links, affecting pointed end depolymerization.

The parameters D, C and $k_-^p(0)$ all depend directly or indirectly on the spacing (ξ) between nucleation promoting factors on the surface of the bead, assuming that all molecules are active. This was previously shown to be true for VCA (Bernheim-Groswasser et al. 2002) and for N-WASP (Wiesner et al. 2003) at an even smaller spacing. The difference between δ and ξ can be justified by the fact that cross-links do not necessarily occur between neighboring filaments. The structural details of actin filament organization in the gel, treated theoretically, for example in Spiros and Edelstein-Keshet (1998), are not developed in the current analysis where cross-linking is characterized only by the mesh size parameter.

Gels around ActA-coated beads are relevant to the situation in the cell. The concentration of ActA on bead surfaces is similar to the density of barbed ends associated with the front face of the lamellipodia in migrating fibroblasts, $\xi = 23$–36 nm (Abraham et al. 1999). In addition, the ActA-generated gel, like the lamellipodia, involves both the Arp2/3 complex and VASP. Thus, the values measured for D, C and $k_-^p(0)$ are biologically meaningful.

The diffusion coefficient for actin monomer in the PRO-produced gel is the same as for the ActA-produced gel, implying that this parameter is dependent only on the interactions of the diffusing actin monomer with actin filaments, and independent of the presence or absence of Arp2/3 and VASP. The elastic modulus of the gel produced by PRO is 100 times larger than the ActA-produced gel. This gives a mesh size value that is three times smaller for the PRO-generated gel, in qualitative agreement with the images in Fig. 1,a, b). In order to estimate the elastic modulus for the NT-produced gel, we use a linear fit of the data in Fig. 4. Owing to the error bars on the large radii beads, this estimate is only representative of the small radii beads where the gel is more regular (Fig. 1e), and we obtain an elasticity value that is comparable to the PRO gel. For larger NT-coated beads the gel appears porous (Fig. 1c), implying that the gel elasticity becomes inhomogeneous with increasing bead radius, and preventing us from interpreting these points ($r \geq 3$ μm) in terms of the stress-limited model. Furthermore, NT-nucleated actin growth does not enter a diffusion-limited regime in the range of bead sizes studied, unlike the ActA and PRO systems, as seen in Fig. 4. This might indicate that diffusion through the NT-produced gel is more rapid, perhaps due to the presence of anfractuosities in the gel. The increased porosity of the NT-produced gel away from the bead surface may explain why comets are not visible for *Listeria* expressing NT in place of ActA in infected cells, despite the fact that these bacteria are motile (Lasa et al. 1997).

Conclusions

Using a well-controlled experimental set-up, we show clear evidence that actin monomer diffusion can play an important role in actin assembly at surfaces. Here, diffusion limits actin gel growth, a restriction that cells might have to over-ride by using other transport mechanisms (Zicha et al. 2003). The values we estimate for the diffusion coefficient of monomers and the elastic moduli of different actin gels are biologically relevant, and corroborate the elastic model for actin gel growth. Our value for the depolymerization rate at the pointed end unveils the important role of reticulation in stabilizing the filaments constituting the gel.

Acknowledgements This work was supported by Curie and CNRS fellowships (J.P.). We thank Vincent Noireaux for performing the treadmilling experiment shown in Fig. 3. We thank Marie-France Carlier for the gift of Arp2/3 and VASP, and Henry Higgs for the p41-Arc antibody.

References

Abraham VC, Krishnamurthi V, Taylor DL, Lanni F (1999) The actin-based nanomachine at the leading edge of migrating cells. Biophys J 77:1721–1732

Bear JE, Svitkina TM, Krause M, Schafer DA, Loureiro JJ, Strasser GA, Maly IV, Chaga OY, Cooper JA, Borisy GG, Gertler FB (2002) Antagonism between Ena/VASP proteins and actin filament capping regulates fibroblast motility. Cell 109:509–521

Bernheim-Groswasser A, Wiesner S, Golsteyn RM, Carlier M-F, Sykes C (2002) The dynamics of actin-based motility depend on surface parameters. Nature 417:308–311

Cameron LA, Footer MJ, Van Oudenaarden A, Theriot JA (1999) Motility of ActA protein-coated microspheres driven by actin polymerization. Proc Natl Acad Sci USA 96:4908–4913

Cameron LA, Svitkina TM, Vignjevic D, Theriot JA, Borisy GG (2001) Dendritic organization of actin comet tails. Curr Biol 11:130–135

Carlier M-F (1998) Control of actin dynamics. Curr Opin Cell Biol 10:45–51

Dogterom M, Yurke B (1997) Measurement of the force–velocity relation for growing microtubules. Science 278:856–860

Drenckhahn D, Pollard TD (1986) Elongation of actin filaments is a diffusion-limited reaction at the barbed end and is accelerated by inert macromolecules. J Biol Chem 261:12754–12758

Eyring H (1935) The activated complex in chemical reactions. J Chem Phys 3:107–115

Fradelizi J, Noireaux V, Plastino J, Menichi B, Louvard D, Sykes C, Golsteyn RM, Friederich E (2001) ActA and human zyxin harbour Arp2/3-independent actin-polymerization activity. Nat Cell Biol 3:699–707

Geese M, Loureiro JJ, Bear JE, Wehland J, Gertler FB, Sechi AS (2002) Contribution of Ena/VASP proteins to intracellular motility of *Listeria* requires phosphorylation and proline-rich core but not F-actin binding or multimerization. Mol Biol Cell 13:2383–2396

Gerbal F, Noireaux V, Sykes C, Jülicher F, Chaikin P, Ott A, Prost J, Golsteyn RM, Friederich E, Louvard D, Laurent V, Carlier M-F (1999) On the *Listeria* propulsion mechanism. Pramana – J Phys 53:155–170

Gerbal F, Laurent V, Ott A, Carlier M-F, Chaikin P, Prost J (2000) Measurement of the elasticity of the actin tail of *Listeria monocytogenes*. Eur Biophys J 29:134–140

Golsteyn RM, Beckerle MC, Koay T, Friederich E (1997) Structural and functional similarities between the human cytoskeletal protein zyxin and the ActA protein of *Listeria monocytogenes*. J Cell Sci 110:1893–1906

Gordon D, Yang Y-Z, Korn E (1976) Polymerization of *Acanthamoeba* actin. Kinetics, thermodynamics and co-polymerization with muscle actin. J Biol Chem 251:7474–7479

Holmes KC, Popp D, Gebhard W, Kabsch W (1990) Atomic model of the actin filament. Nature 347:44–49

Isambert H, Venier P, Maggs AC, Fattoum A, Kassab R, Pantaloni D, Carlier M-F (1995) Flexibility of actin filaments derived from thermal fluctuations. J Biol Chem 270:11437–11444

Kabsch W, Mannherz HG, Suck D, Pai EF, Holmes KC (1990) Atomic structure of the actin:DNase I complex. Nature 347:37–44

Käs J, Strey H, Tang JX, Finger D, Ezzell R, Sackmann E, Janmey PA (1996) F-actin, a model polymer for semiflexible chains in dilute, semidilute, and liquid crystalline solutions. Biophys J 70:609–625

Kocks C, Gouin E, Tabouret M, Berche P, Ohayon H, Cossart P (1992) *L. monocytogenes*-induced actin assembly requires the *actA* gene product, a surface protein. Cell 68:521–531

Kramers HA (1940) Brownian motion in a field of force and the diffusion model of chemical reactions. Physica (Utrecht) 7:284–304

Landau L, Lifchitz E (1976) Statistical physics, 3rd edn. Mir, Moscow

Lanni F, Ware BR (1984) Detection and characterization of actin monomers, oligomers, and filaments in solution by measurement of fluorescence photobleaching recovery. Biophys J 46: 97–110

Lasa I, Gouin E, Goethals M, Vancompernolle K, David V, Vandekerckhove J, Cossart P (1997) Identification of two regions in the amino terminal domain of ActA involved in the actin comet tail formation by *Listeria monocytogenes*. EMBO J 16:1531–1540

Laurent V, Carlier M-F (1998) Use of platelet extracts for actin-based motility of *Listeria monocytogenes*. In: Celis J (ed) Cell biology: a laboratory handbook, vol 2. Academic Press, Toronto, pp 359–365

Luby-Phelps K, Taylor DL, Lanni F (1986) Probing the structure of cytoplasm. J Cell Biol 102:2015–2022

Luby-Phelps K, Castle PE, Taylor DL, Lanni F (1987) Hindered diffusion of inert tracer particles in the cytoplasm of mouse 3T3 cells. Proc Natl Acad Sci USA 84:4910–4913

Machesky LM (2002) Sharks' teeth and dunes. Nature 417:494–495

Machesky LM, Insall RH (1999) Signaling to actin dynamics. J Cell Biol 146:267–272

McGrath JL, Tardy Y, Dewey CF Jr, Meister JJ, Hartwig JH (1998) Simultaneous measurements of actin filament turnover, filament fraction, and monomer diffusion in endothelial cells. Biophys J 75:2070–2078

Mogilner A, Edelstein-Keshet L (2002) Regulation of actin dynamics in rapidly moving cells: a quantitative analysis. Biophys J 83:1237–1258

Mullins RD, Heuser JA, Pollard TD (1998) The interaction of Arp2/3 complex with actin: nucleation, high affinity pointed end capping, and formation of branching networks of filaments. Proc Natl Acad Sci USA 95:6181–6186

Noireaux V (2000) Etude d'un système biomimetique de *Listeria*. Université Paris XI, Paris

Noireaux V, Golsteyn RM, Friederich E, Prost J, Antony C, Louvard D, Sykes C (2000) Growing an actin gel on spherical surfaces. Biophys J 278:1643–1654

Ölveczky BP, Verkman AS (1998) Monte Carlo analysis of obstructed diffusion in three dimensions: application to molecular diffusion in organelles. Biophys J 74:2722–2730

Pollard TD (1986) Rate constants for the reactions of ATP- and ADP-actin with the ends of actin filaments. J Cell Biol 103:2747–2754

Pollard TD, Blanchoin L, Mullins RD (2000) Molecular mechanisms controlling actin filament dynamics in nonmuscle cells. Annu Rev Biophys Biomol Struct 29:545–576

Reinhard M, Halbrügge M, Scheer U, Wiegand C, Jockusch BM, Walter U (1992) The 46/50 kDa phosphoprotein VASP purified from human platelets is a novel protein associated with actin filaments and focal contacts. EMBO J 11:2063–2070

Robinson RC, Turbedsky K, Kaiser DA, Marchand J-B, Higgs HN, Choe S, Pollard TD (2001) Crystal structure of Arp2/3 complex. Science 294:1679–1684

Skoble J, Portnoy DA, Welch MD (2000) Three regions within ActA promote Arp2/3 complex-mediated actin nucleation and *Listeria monocytogenes* motility. J Cell Biol 150:527–537

Skoble J, Auerbuch V, Goley ED, Welch MD, Portnoy DA (2001) Pivotal role of VASP in Arp2/3 complex-mediated actin nucleation, actin branch-formation, and *Listeria monocytogenes* motility. J Cell Biol 155:89–100

Spiros A, Edelstein-Keshet L (1998) Testing a model for the dynamics of actin structures with biological parameter values. Bull Math Biol 60:275–305

Sutherland JD, Way M (2002) Looking over the edge: a new role for Ena/VASP proteins in lamellipodial dynamics. Dev Cell 2:692–694

Svitkina TM, Borisy GC (1999) Arp2/3 complex and actin depolymerizing factor/cofilin in dendritic organization and treadmilling of actin filament array in lamellipodia. J Cell Biol 145:1009–1026

Theriot JA, Fung DC (1998) Use of *Xenopus* egg extracts for studies of actin-based motility, vol 2, 2nd edn. Academic Press, New York

Theriot JA, Mitchison TJ, Tilney LG, Portnoy DA (1992) The rate of actin-based motility of intracellular *Listeria monocytogenes* equals the rate of actin polymerization. Nature 357:257–260

Wiesner S, Helfer E, Didry D, Ducouret G, Lafuma F, Carlier M-F, Pantaloni D (2003) A biomimetic motility assay provides insight into the mechanism of actin-based motility. J Cell Biol 160:387–398

Zicha D, Dobbie IM, Holt MR, Monypenny J, Soong DYH, Gray C, Dunn GA (2003) Rapid actin transport during cell protrusion. Science 300:142–145